Separation of the Nonlinear Oscillatory Response into a Superposition of Linear, Strain Hardening, Strain Softening, and Wall Slip Response

Christopher O. Klein,[†] Hans W. Spiess,[†] Andreea Calin,[†,§] Corneliu Balan,[§] and Manfred Wilhelm*[,†,‡]

Max Planck Institut für Polymerforschung, Ackermannweg 10, 55021 Mainz, Germany, Institut für Technische und Polymerchemie Universität Karlsruhe, 76128 Karlsruhe, Germany, and "Politehnica" University of Bucharest, 060042 Bucharest, Romania

Received October 23, 2006; Revised Manuscript Received March 28, 2007

ABSTRACT: Water-based dispersions and emulsions are used as model systems for a new rheological data analysis. The application of large amplitude oscillatory shear can be used to generate a high nonlinear response, which is analyzed by Fourier transform (FT)-rheology. The individual higher harmonics appearing in the shear stress response do not have a simple physical interpretation. Furthermore, in the FT analysis used so far the focus was mainly on the third harmonic relative to the fundamental I_3/I_1, even if multiple higher harmonics appear, as in the polystyrene dispersions examined here. As a consequence, we propose a new and simple method that considers the whole overtone spectra as a superposition of different overtone spectra of typical nonlinear rheological effects, like strain hardening, strain softening, and shear bands or wall slip. This novel analysis of FT-rheology experiments thus separates the nonlinear mechanical response into the underlying physical phenomena.

Introduction

During the production and processing of materials, the nonlinear mechanical regime is omnipresent at a large scale. Additionally, complex fluids show a great variety of rheological properties.[1,2] For the processing, it is important to understand the relation between the shear-induced structures (e.g., of dispersions) and the nonstationary nonlinear mechanical properties. The appearance of odd higher harmonics in the oscillatory shear stress response are well established[3−8] and can be analyzed with Fourier transform (FT)-rheology. The application of large amplitude oscillatory shear (LAOS) is used to generate and to describe the nonlinear behavior.[8−11] However, the analysis of nonlinear oscillatory mechanical data with respect to the amplitudes and the phases[12] of the higher harmonics does not always result in a simple physical picture or interpretation. Furthermore, the analysis of nonlinear oscillatory data is often focused on the magnitude I_3/I_1 and the phase of the third harmonic Φ_3. In many cases, this analysis is justified because only the intensity of the first harmonics (e.g., third, fifth) are large enough to be analyzed. However, in the hard-sphere model systems examined here, a large number of higher harmonics of the excitation frequency with high intensity are detected, up to the 45th harmonic. Moreover, in such samples not only odd harmonics but even harmonics at $2\omega_1$, $4\omega_1$, etc. are observed as well. These even harmonics should not be neglected because their intensities are larger than 1%, and their intensity is very reproducible (see Figure 1). Thus, if only the third harmonic is considered, important information is neglected. Therefore, an extension of the analysis of data obtained via FT-rheology is required. The extension presented here considers the whole frequency spectrum as a superposition of different overtone subspectra of typical characteristic nonlinear rheological effects, such as linear response, strain hardening, strain softening, and shear bands or wall slip. In the following, the functions used to describe these known rheological phenomena will be called characteristic functions. The quantification of the nonlinear response with respect to these characteristic functions is based on the determination of the magnitude of the higher harmonics (I_n/I_1), relative to the fundamental, and the determination of the corresponding phases Φ_n. This novel analysis, based on FT-rheology experiments, gives an easy access to the quantification of the nonlinear mechanical regime with respect to strain hardening, softening, and shear bands.

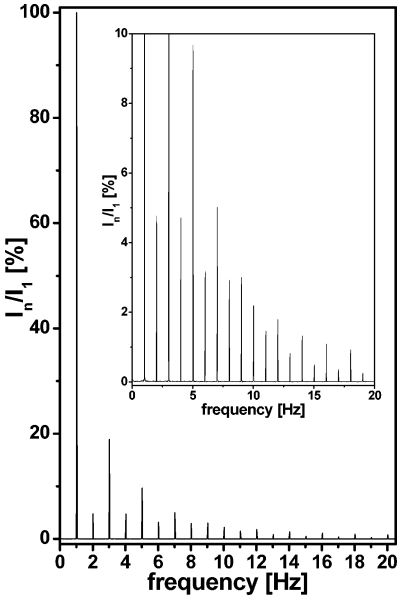

Figure 1. FT magnitude spectra of sample 2 at an excitation frequency of $\omega_1/2\pi = 1$ Hz, strain amplitude $\gamma_0 = 0.5$, and a temperature of 293 K. The inset shows the zoom-in on the higher harmonics.

Experimental Procedures

Apparatus. The FT-rheology setup used consists of a Rheometrics Scientific advanced rheometer expansion system (ARES)

* To whom correspondence should be addressed. E-mail: wilhelm@polymer.uni-karlsruhe.de. Tel: +49 721 608 3150. Fax: + 49 721 608 3153.
[†] Max Planck Institut für Polymerforschung.
[‡] Institut für Technische und Polymerchemie Universität Karlsruhe.
[§] "Politehnica" University of Bucharest.

10.1021/ma062441u CCC: $37.00
Published on Web 05/16/2007

Table 1. Characterization of Samples Using Particle Dispersity Index, Solid Content, and Particle Diameter of Samples 1 and 2

	sample 1	sample 2
monomer	styrene, acrylic acid	styrene, buthylmethacrylate (wt ratio 1:1), acrylic acid
PDI	1.04	1.01
solid content [%]	35.4	32.7
particle diameter [nm]	69.7	133.2

and two computers. The ARES rheometer is a strain-controlled rheometer equipped with a dual range force rebalance transducer (100 FRTN1) capable of measuring torques ranging from 0.004 to 10 mNm. It has a high resolution motor, applying frequencies from 10^{-5} to 500 rad/s and deformation amplitudes ranging from 0.005 to 500 mrad. The temperature range of the water bath is from −20 to 95 °C. A first computer (PC) controls the rheometer via a serial cable. The strain, torque, and normal force outputs are connected to a second computer via BNC cables, where the data for the FT-rheology is acquired, digitized, and analyzed via a 16-bit ADC-card (PCI-MIO-16XE-10 from National Instruments, USA). The maximum sampling rate of this card is 100 kHz, and it is capable of multiplexing up to 16 channels. It can simultaneously acquire and transfer the data to the PC memory by data-buffering techniques. Therefore, the rheological data is intrinsically synchronized. After acquisition, the time data is averaged on-the-fly and subsequently Fourier transformed using home-written Lab VIEW software programs.[12,13] In the experiments, a double wall Couette cell was used. The cup has a slit diameter between 27 and 34 mm and a bob diameter between 29 and 32 mm.

The size of the particles and the size distribution are measured via dynamic light scattering with a Malvern Zetasizer 5000. The incorporated correlator is of the type 7132 with 62 correlation channels. The light source is a 5 mW HeNe-LASER at a wave length, $\lambda = 633$ nm.

Materials. The dispersions are synthesized via a mini-emulsion polymerization, which is a radical polymerization.[14] The mini-emulsions are stabilized monomer droplets (including a hydrophobic agent) with a size between 50 and 500 nm in a continuous water phase. They are prepared by high-frequency ultrasonication of a system containing monomer, water, a surfactant, and a hydrophobic agent (e.g., hexadecane). The interaction between the droplets (e.g., Ostwald ripening or coalescence) is suppressed by the hydrophobic agent and a low molecular weight surfactant (e.g., sodium dodecyl sulfate (SDS) is used). The polymerization proceeds only in these droplets ("nanoreactors") and generates nanoparticles of the same size as the initial droplets. The size of the droplets can be adjusted in a controlled way via duration and power of the ultrasonication. The homogeneous size distribution of the emulsions is enforced by the use of a hydrophobic agent.[14]

For the sample preparation, two mixtures are made in separate beakers. The first contains 50 g of water, 0.4 g of the surfactant SDS, 0.1 g of the initiator azo-*bis*-isobutyronitrile. The second beaker contains 30 g of monomer (sample 1, 30 g styrene; sample 2, 15 g styrene and 15 g buthylmethacrylate), 0.5 g of the hydrophobe hexadecane, and 0.1 g of acrylic acid. After mixing these two beakers and stirring for 1 h, the solution was mixed with a Branson digital sonifier model 250-D with a resonator 0.5 in. (W-250) for 2 min at an amplitude of 89%. The reactive medium is cooled during the sonication. Afterward, the mixture is taken to the reactor, and the synthesis is performed at 72 °C for 12 h.

The dispersions synthesized by mini-emulsion polymerization have Debye lengths that range from 1.7 to 1.8 nm. The Debye-length λ is the characteristic length,[15] which describes the screening distance of a central ion potential by a cloud of surrounding ions. The solid contents of the synthesized dispersions range from 35 to 60 wt. %. The diameter of the particles ranges from 70 to 250 nm and particle dispersity index (PDI) ranges from 1.01 to 1.04. For the properties of the samples examined, see Table 1.

Experiments. The rheological experiments cover the range from the linear to the nonlinear regime. The conducted measurements are variations of the shear rate (steady shear), the frequency at constant strain amplitude, and variations of the strain at a constant frequency (both dynamic shear). Especially in the nonlinear regime, measurements where frequency and strain amplitudes were varied are applied.

For light scattering measurements, the dispersions are diluted with "Millipore water". The resulting solid content must not be higher than 0.1 wt. % to avoid multiple scattering. About 5 mL are filled in the measurement cuvette and analyzed.

The solid content of the dispersions is determined via gravimetric analysis. About 2 g of the dispersion is put in an aluminum jacket and the volatile parts are evaporated under vacuum. The dispersions are heated for 12 h at 60 °C in a vacuum of 100 mbar prior to gravimetric analysis.

For the rheological measurements, an appropriate amount (e.g., 10 mL) of the sample is filled into the Couette cell. A solvent trap is used to prevent evaporation. This trap is equipped with a sponge drawn with water. A thin dodecane-layer ($C_{12}H_{26}$) covers additionally the solution to prevent an exchange with the atmosphere above. Dodecane is nonpolar and with a viscosity of 1.4 mPa s[16] has a lower viscosity than the samples with a high-particle loading. Following an initiation of about 10 oscillations, typically 40 oscillations have been acquired, while an Analog Digital Converter (ADC) scanning rate of 50 000 1/s for each channel and an oversampling of 1,000[13] raw data points are typically selected. This procedure results in 50 preaveraged data points per second, which is sufficient for the purposes of the experiments conducted here.

Principle of the New Data Analysis

A simple physical interpretation of the results of the nonlinear oscillatory mechanical data with respect to the amplitudes and the phases of the higher harmonics is not always possible.[12,17] This is also true for dispersions under LAOS studied here. Therefore, a new interpretation of the FT-rheology, which considers the whole frequency spectrum as a superposition of different overtone spectra of typical nonlinear rheological effects, was developed. These rheological archetypes are described by characteristic response functions. The total response can then simply be described by a superposition of these functions, and their relative contributions quantify the nonlinear response. The response is considered to be a superposition of linear and nonlinear contribution with varying amount. To make the transition from linear to the high nonlinear regime, this amount starts from zero and monotonically increases. For simplicity, only four rheological effects are considered (one linear and three nonlinear): linear response, strain hardening, strain softening, and stick-slip as being the most important ones, under LAOS conditions. The suggested analysis is based on the determination of the magnitude of the higher harmonics (I_n/I_1), relative to the fundamental, and the determination of the corresponding phases ϕ_n of the generated higher harmonics. The response is considered to be a superposition of linear and nonlinear contribution with varying amount. To make the transition from linear to the highly nonlinear regime, this amount starts from zero and monotonically increases.

Within this article we would like to use the term shear thinning/thickening, respectively, for the shear rate dependent viscosities and strain softening/hardening, respectively, for the strain amplitude dependent complex viscosities. In case a system adjusts infinitely fast to the applied excitation, the meaning of the two terms is the same.

The measured signal can then be fitted both in the time or the frequency domain with up to four characteristic contributions, (Figure 2a). In Figure 2b, the corresponding magnitude spectrum is shown. These characteristic contributions are a

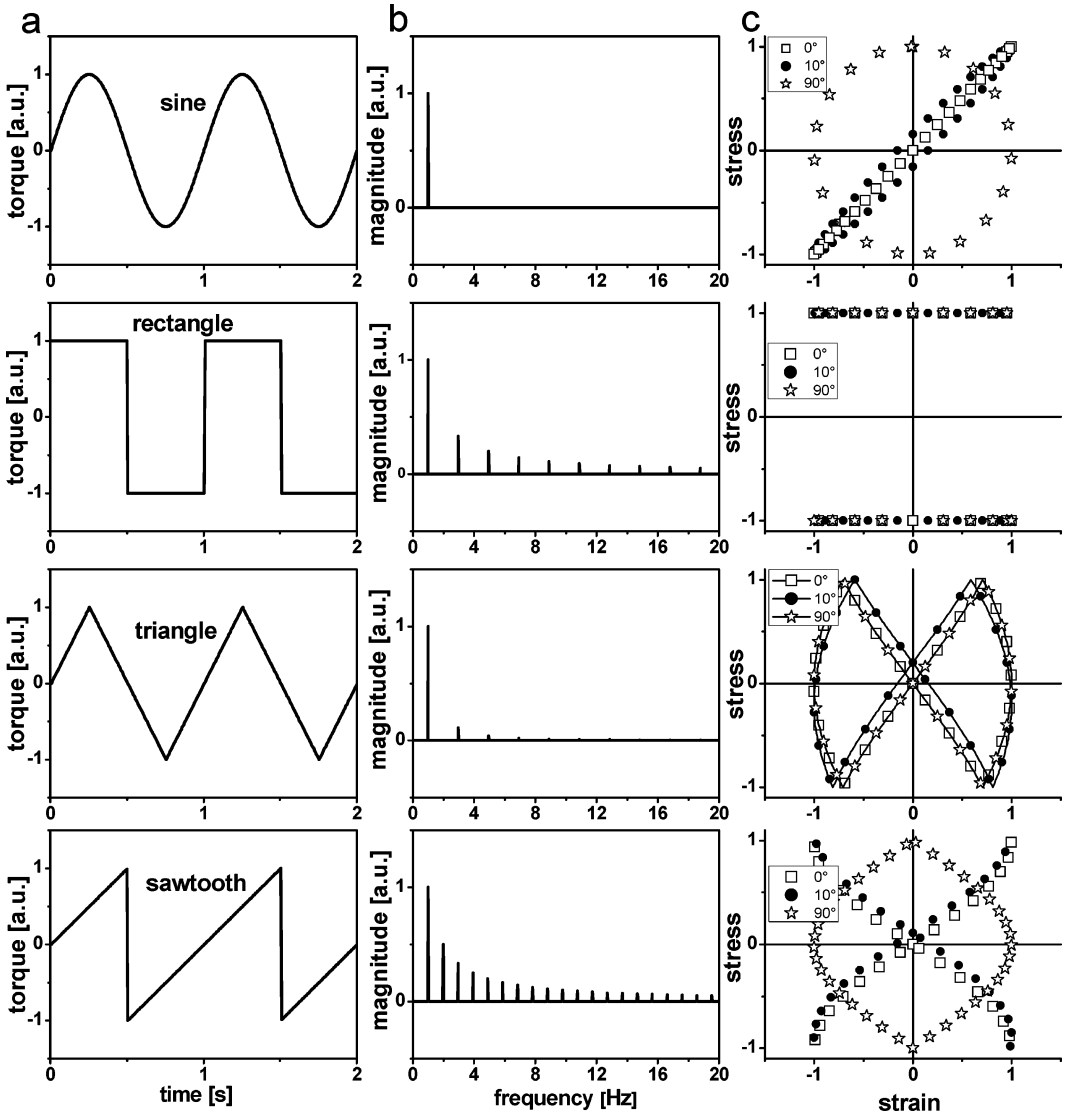

Figure 2. The four characteristic functions (from top to bottom): a sine, a rectangular, a triangular, and a saw tooth shaped wave, representing linear behavior, strain softening, strain hardening, and shear bands, respectively. Time domain data (a) and the corresponding FT magnitude spectra (b). For a better understanding, the Lissajou figures of the characteristic functions were added on (c), each plot with a phase difference of 0°, 10°, and 90° relative to a sinusoidal excitation.

sinusoidal function (see eq 1), describing the linear response, a rectangular function (see eq 2), describing strain softening, a triangular function (see eq 3), describing strain hardening, and finally a saw tooth function (see eq 4), describing shear bands or wall slip. Each one of these functions can be varied 2-fold with respect to the others via the amplitude and the relative time lag (phase lag). In Figure 2c, the classical Lissajou figures are plotted for phase differences of 0°, 10°, and 90°. The sinusoidal wave is selected for the linear response because it describes the behavior in the linear regime. The specific functions for shear thickening (triangular wave) and shear thinning (rectangular wave) are used because they resemble the shape of this type of response.[12] This choice is not unique, but most simple. To quantify wall slip or stick slip, the saw tooth wave is selected, because it describes a periodic signal that alternates between increasing torques and slip (sudden drop in torque). These nonlinear characteristic functions are the limiting cases for the maximum possible nonlinearities of strain hardening, strain softening, and shear bands. For convenience of the reader, the Fourier series of these characteristic functions are reproduced.[18,19] Note that these functions contain specific amplitudes and phases.

The linear response is given by

$$\sigma_l(t) = A_l \sin(\omega_1 t + \delta_l) \tag{1}$$

The periodic rectangular function is given by

$$\sigma_r(t) = A_r \frac{4}{\pi}\left(\sin(\omega_1 t + \delta_r) + \frac{\sin 3(\omega_1 t + \delta_r)}{3} + \frac{\sin 5(\omega_1 t + \delta_r)}{5} + ...\right) \tag{2}$$

The periodic triangular function is given by

$$\sigma_t(t) = A_t \frac{4}{\pi}\left(\sin(\omega_1 t + \delta_t) - \frac{\sin 3(\omega_1 t + \delta_t)}{3^2} + \frac{\sin 5(\omega_1 t + \delta_t)}{5^2} - ...\right) \tag{3}$$

The periodic saw tooth is given by

$$\sigma_{st}(t) = A_{st}2\left(\sin(\omega_1 t + \delta_{st}) - \frac{\sin 2(\omega_1 t + \delta_{st})}{2} + \frac{\sin 3(\omega_1 t + \delta_{st})}{3} - ...\right) \quad (4)$$

The superimposed total signal is given by

$$\sigma(t) = \sigma_l(t) + \sigma_r(t) + \sigma_t(t) + \sigma_{st}(t) \quad (5)$$

By superimposing these different contributions (see eq 5), the measured time domain signal of the torque response is reconstructed. Additionally, the measured torque signal is analyzed in frequency space with respect to the higher harmonics intensities I_n/I_1 and phases ϕ_n. This is of special importance for low-intensity contributions of the higher harmonics or for optimization of the fits. Both the reconstructed time data and the FT analysis of the experimental and reconstructed signal are used to determine the different contributions of strain softening and hardening. In several cases, even harmonics appear, which are described by a saw tooth function, and might be caused by shear bands, wall slip, and disaggregation or yield effects. The superposition of these four functions results in a time response that should mimic the measured time domain signal. Because the time signal is rather complex, the reconstructed signal has to be adapted by changing the relative phases (time lag) and magnitude of each of the four overlaying functions (sine, rectangular, triangular, saw tooth) with respect to each other. The parameters A_r, A_t, A_{st} are relative to the value of $A_l = 1$. The phases of the different contributions are relative to the phase of the ϕ_l (the phase of the linear contribution).

After Fourier transformation, the magnitudes and the phases of the simulated and of the measured signal should ideally be identical, within the reproducibility of the experiment, and the time response should perfectly overlay.

Experimental Example. For a better visualization and understanding of this new concept the Fourier spectra of the proposed characteristic functions are now discussed (see Figure 2). The linear contribution, a sine wave, results in a spectrum with one peak at the excitation frequency only. The strain softening contribution, a rectangular function, and the strain hardening wave, a triangular function, show only peaks at odd higher harmonics of the excitation frequency. One main difference between these two functions is the decrease (envelope function) of the intensity of the higher harmonics with increasing frequencies. The intensities of the higher harmonics decrease in the case of strain softening with $1/n$ ($n = 1, 3, 5...$) and in the case of strain hardening with $1/n^2$ ($n = 1, 3, 5...$). Besides this, the phase of the higher harmonics is obviously different. For the rectangular function the phases of the higher harmonics are the same (for $\delta_r = 0$), for the triangular function they alternate between 0 and π (for $\delta_l = 0$). The fourth characteristic function is used to mimic shear bands or wall slip contributions with a saw tooth wave. This contribution has higher harmonics at even and odd multiples of the excitation frequency. The intensity decreases with a factor of $1/n$ ($n = 1, 2, 3...$).

The superposition of the different contributions can then result both in an increase or a decrease of the intensity of harmonics, depending on the phase lag between the different contributions, analogous to constructive and destructive interference of waves (e.g., in optics). The phase lags between the different contributions enter into the total phase of the higher harmonics. As an example, the behavior of the phase and the magnitude of the third harmonics originating from a superposition of a rectangular function and a saw tooth function are simulated. The values for the intensity of the third harmonic and phase of the third harmonic are listed depending on the phase lag between the rectangular function and the saw tooth wave (see Table 2). Clearly the phase lag has a pronounced influence on the values of the intensities and phases. Therefore, these amplitudes and phases themselves have no simple physical meaning.

Table 2. Superposition of a Rectangular Function and a Saw Tooth Function[a]

phase lag characteristic functions [°]	I_3/I_1 [%]	Phase Φ_3 [°]
0	33.3	180
110	51	82
140	63	116
180	33.3	180

[a] The resulting intensities and phases of the third harmonic, depending on the phase lag between the rectangular function and the saw tooth function, are presented. The amplitudes are the same for both the rectangular ($4/\pi A_r = 1$) and the saw tooth function ($2A_{st} = 1$).

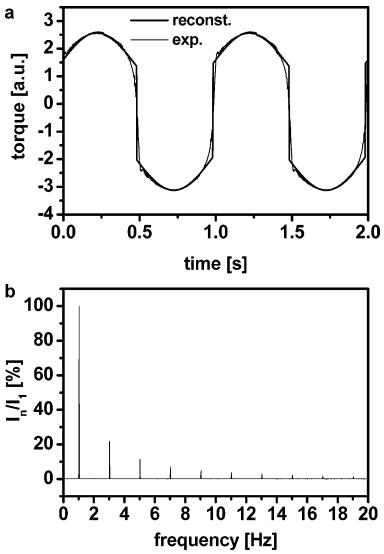

Figure 3. The overlay of the torque response and the reconstructed data of the sample 1 (a) and the corresponding FT magnitude spectra of the experimental data (b). The time domain signals were recorded at 298 K with $\omega_1/2\pi = 1$ Hz and $\gamma_0 = 1$.

Results and Discussion

The simple functions considered here are limits for ultimate shear thinning, hardening, etc. This generates sharp edges and cusps, which of course are not observed in the experiment, with finite response times and a given inertia.

For illustration, sample 1 and sample 2 were analyzed under LAOS conditions using the concept of these characteristic functions. The overlay of the measured data and the reconstructed data for sample 1 and sample 2 is shown in Figures 3a and 4a, respectively. The magnitude spectra of sample 1 and sample 2 are presented in Figures 3b and 4b. The measured data and the reconstructed data overlay well in the maxima, but deviations between measured and reconstructed data show up around the turning point (stress = 0) of the periodic functions. The different contributions of the four characteristic functions, their amplitudes, their phases, and their time lags, are presented in Table 3 for sample 1 and in Table 4 for sample 2. The amplitudes of the characteristic functions A_r, A_t, and A_{st} are normalized with respect to A_l. The time lag is derived from the phase shift between the linear contribution and the strain softening or shear band contribution. The triangular function was not used because the system showed only shear thinning

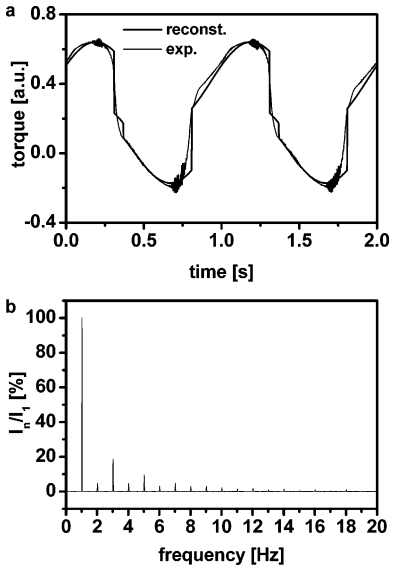

Figure 4. The overlay of the torque response and the reconstructed data of the sample 2 (a) and the corresponding FT magnitude spectra of the experimental data (b). The time domain signals were recorded at 298 K with $\omega_1/2\pi = 1$ Hz and $\gamma_0 = 6$.

Table 3. Frequency, Intensity, and Phase of the Characteristic Functions of the Reconstructed Response of Sample 1 (See Figure 3a)

	frequency [Hz]	normalized amplitude	phase [°]	time-lag [ms]
sinusoidal	1	1	0	0
rectangular	1	1.47	35	97
saw tooth	1	< 0.01	*a*	*a*

[a] Below accuracy.

Table 4. Frequency, Intensity, and Phase of the Characteristic Functions of the Reconstructed Response of Sample 2 (See Figure 4a)

	frequency [Hz]	normalized amplitude	phase [°]	time lag [ms]
sinusoidal	1	1	0	0
rectangular	1	1.4	51	142
saw tooth	1	0.36	∼0	∼0

Table 5. Magnitudes and the Phases from the Measurements and the Reconstruction of Sample 1 (Figure 3)

harmonics	2.	3.	4.	5.	6.	7.
measured magnitude [%] I_n/I_1	0.2	21.8	0.1	11.3	0.1	7.2
reconstructed magnitude [%] I_n/I_1	0.0	21.7	0.0	13.0	0.0	9.3
measured phase [°]	64	177	266	351	141	163
reconstructed phase [°]	76	177	27	356	41	175

Table 6. Magnitudes and the Phases from the Measurements and the Reconstruction of Sample 2 (Figure 4)

harmonics	2.	3.	4.	5.	6.	7.
measured magnitude [%]	4.7	19.4	4.7	9.7	3.2	4.9
reconstructed magnitude [%]	4.0	19.4	2.0	12.3	1.3	10.3
measured phase [°]	214	236	76	92	305	305
reconstructed phase [°]	231	236	87	108	101	325

behavior. Note the dramatic differences between both time and frequency data of the two samples that in our analysis is easily identified as being due to the big difference in the saw tooth contribution.

For a better comparison between the measured and reconstructed data, both magnitudes and phases (of measured and reconstructed data) of sample 1 (Table 5) and sample 2 (Table 6) are presented for the higher harmonics also. Good agreement, typically within less than 1% relative deviation is found for I_2/I_1, I_3/I_1, and I_5/I_1 in the magnitude spectra. For $\Phi_{2/1}$, $\Phi_{3/1}$, and $\Phi_{5/1}$, the values for the phase give also very reasonable results, generally within less than $\pm 10°$. For very high order harmonics I_n/I_1, the agreement is still highly satisfactory where the phases of the very weak overtones should, of course, not be considered.

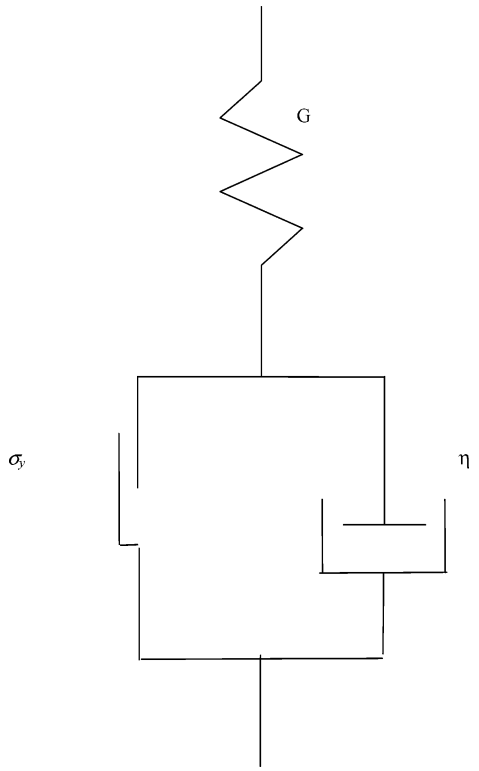

Figure 5. Schematic representation of the Bingham material.

To verify the validity of this new method, we have applied it to a nonlinear response obtained through by numerically solving the equation that describes the Bingham[1,2] model (see Figure 5)

$$\dot{\gamma}(t) = \frac{\dot{\sigma}(t)}{G} + U(\sigma(t) - \sigma_y)\frac{\sigma(t) - \sigma_y}{\eta} + U(-\sigma(t) - \sigma_y)\frac{\sigma(t) + \sigma_y}{\eta} \quad (6)$$

where G is the spring modulus, η is the dashpot viscosity, σ_y is the yield stress, $U(x)$ is the step function of x ($U(x) = 0$ for $x < 0$, $U(x) = 1$ for $x > 0$.

It is well understood that the nonlinearity of this equation results from the yield stress that implicitly leads to shear thinning. For strain amplitudes that do not exceed the critical value $\gamma_c = \sigma_y/G$, the material response is linear. The nonlinearity appears when the stress exceeds σ_y and decreases progressively when the strain amplitude becomes large enough, thus, when the yield stress has reduced influence. The shear thinning is important in the vicinity of γ_c, because the slope of the flow curve is decreased to η from infinity.

In the numerical simulations we have used the values $G = 0.1$ Pa, $\sigma_y = 0.4$ Pa, and $\eta = 0.01$ Pa·s and applied a sinusoidal strain $\gamma(t) = \gamma_0 \sin(\omega_1 t)$, with γ_0 of 3, 30, and 300 respectively. The numerical solution of the Bingham one-dimensional constitutive eq 6 were fitted with eq 5. The results are shown in Figure 6 where the dotted line represents the excitation, the dashed line is the material response (obtained from eq 6), and the continuous line shows the fit according to eq 5.

The values of the resulted parameters are shown in Table 7. By analyzing the prefactors that result from the fit (see eqs 2−6),

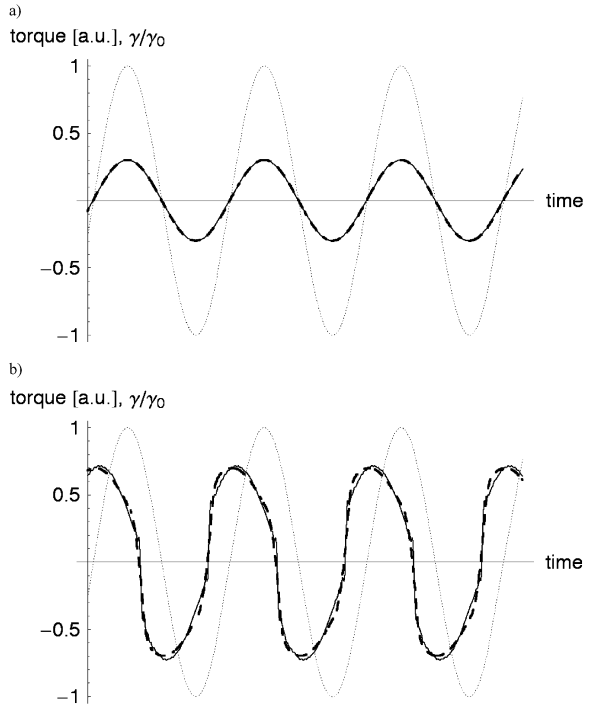

Figure 6. Excitation (dotted line), fit (continuous line), and response (dashed line) of a Bingham material described by eq 6, with $\omega_1 = 1$ Hz, $G = 0.1$ Pa, $\sigma_y = 0.4$ Pa, and $\eta = 0.01$ Pa·s, $\gamma_c = 4$. (a) $\gamma_0 = 3$; (b) $\gamma_0 = 30$.

Table 7. Fitting Parameters for a Bingham Material Subjected to LAOS

strain amplitude γ_0	normalized rectangular amplitude	rectangular phase [°]	normalized saw tooth amplitude	saw tooth phase [°]
3	0	212.4	0	48.6
30	0.2	163.8	0.09	214.2

the normalized rectangular amplitude and the normalized saw tooth amplitude, respectively, we can conclude that the nonlinear behavior observed in the Bingham material results from the shear thinning and yield stress, like the constitutive eq 6 predicts.

Current Limitations. As noted above, the reason for this increasing lack of precision for the higher harmonics is the simplification using the rectangular wave for modeling the shear thinning behavior. The here applied, but not unique, step function has an infinite steep slope that results in very sharp flanks in the resulting reconstructed signal. A trapezoidal function or the folding with a Gaussian function in the time domain data could help to reduce the deviations, because these measures would result in a less steep slope on the flanks. Similarly, the sharp cutoff in the saw tooth function should be smoothed. Generally, the intensities of the reconstructed higher harmonics are somewhat higher than the measured ones. This is also a consequence of the simplification (sinusoidal, rectangular, triangular, and saw tooth shape) containing sharp edges and therefore increases the nonlinearities of the characteristic functions. Obviously, these maximum nonlinearities are rarely reached within real materials. Simple multiplication with, for example, a Gaussian function, in the reconstructed FT-spectra might therefore be used to get a better agreement for the higher harmonics intensities. This multiplication in frequency space is equivalent to a Gaussian convolution in the time domain. On the other hand, such a multiplication would introduce new parameters and therefore would weaken the simplicity of our approach at this point.

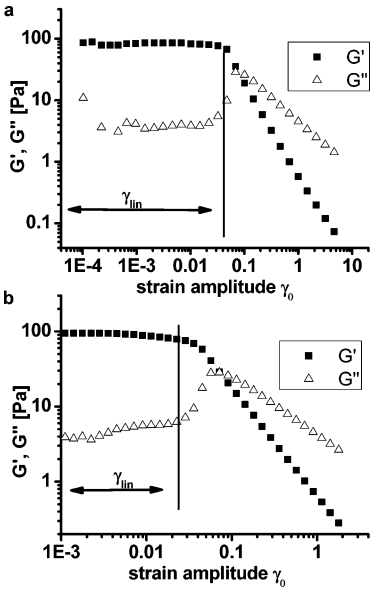

Figure 7. Strain sweep at a frequency $\omega_1/2\pi = 1$ Hz and a temperature of 293 K for dispersion sample shown in 1 (a) and sample displayed in 2 (b). No overshoot is found in G′ but is found in G″. The sample response is typical for Ahn type III.[10] For $\gamma_0 < 0.01$ respectively $\gamma_0 < 0.06$, the samples respond linear using this method. At higher strain amplitudes, the samples display strain softening.

Irrespective of the minor problems related to the higher-order intensities, the phase of a third harmonic ϕ_3 can now be interpreted as a superposition of different contributions. This phase ϕ_3 can then be analyzed by a superposition of a third harmonic originating from a strain softening process and a shear banding process in the sample. These different processes have furthermore a phase related to the time lag of these different contributions, as seen in Table 3 for sample 1 and Table 4 for sample 2 (see eqs 1−4).

The analysis proposed here could in principle be applied to the numerical solutions of all nonlinear constitutive equations. Even so, the reader should be aware that the general structure of the nonlinear constitutive equation does not provide a unique and inherent separation in the proposed four contributions. Nevertheless, these contributions seem to be the simplest functions that reflect the underlying processes. Obviously, further progress can be done along these lines.

Dependence on Strain Amplitude. In a following step, this new analysis of the mechanical response was then applied to a whole data set of oscillatory response signals that differ in the applied strain amplitudes. In a strain sweep, these samples show an overshoot in G″ (see Figure 7 a,b). This is type III behavior according to the nomenclature introduced by Ahn.[9] The dependence of the amplitude and phase with respect to the strain amplitude is represented in Figure 8a,b for sample 1 and Figure 9a,b for sample 2. In Tables 8 and 9, the values for the amplitudes and phases of the rectangular function and the saw tooth function of the samples 1 and 2 are given. The values of the amplitudes are normalized with respect to the amplitude of the pure sinusoidal function. The phase values of the rectangular, triangular, and saw tooth function are relative to a phase of the sine function phase of 0°. The sinusoidal response was used as reference with the amplitude set to $A_l = 1$ and a phase angle $\delta_l = 0$. The amplitudes of the characteristic functions A_r, A_t, and A_{st} are normalized with respect to A_l.

For both samples, three characteristic functions for the linear response, strain softening, and wall slip are needed to obtain a satisfactory match to the experimental data, in particular at high

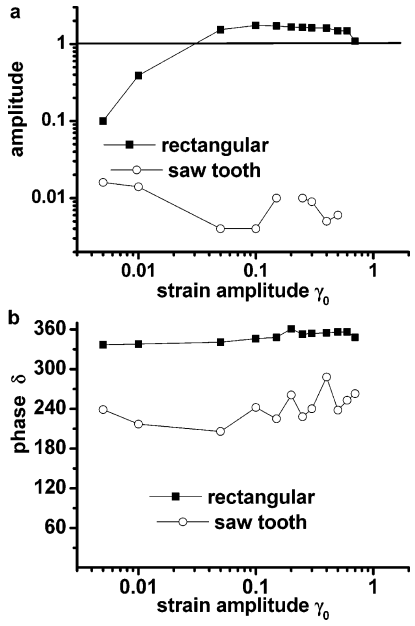

Figure 8. Dependence of the amplitude and the phase on the strain amplitude of the characteristic functions of the sample 1. The characteristic response contains strain softening and wall slip or shear bands. In rare cases, experimental problems, such as wall slip, appeared. In those cases, the data is not shown.

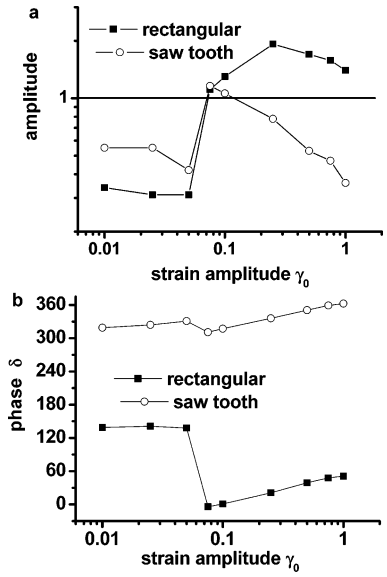

Figure 9. Dependence of the amplitude and the phase on the strain amplitude of the characteristic functions of the sample 2. The characteristic response is a superposition of strain softening and wall slip or shear bands.

strain amplitudes. The triangular function, describing the strain hardening, was not needed in the reconstruction as no strain hardening could be detected in the samples. With increasing γ_0, the amplitude of the rectangular function increased until a maximum was reached. This dependence of the amplitude resembles the typical behavior of the intensity of the third harmonic as an approximately good fit function of γ_0^7 for small γ_0. For sample 1, the amplitude of the saw tooth function is considerably lower compared with the rectangular function (please note the double logarithmic scale). The phases of the two functions show a small tendency to increase with increasing γ_0, but the distance between both is almost constant. The phase of the rectangular function is about 360°, therefore in-phase with the linear contribution. About 20 dispersions were synthesized and were found to respond in a similar way.

An exception to this finding is the behavior of sample 2. It shows even at $0.01 < \gamma_0 < 0.06$, there are always nonlinearities in the range of A_r 0.3 and A_{st} 0.6, respective I_n/I_1 0.4 (see Figure 9). In fact, at small γ_0 values the saw tooth function is larger in amplitudes than the rectangular function. At a value of $\gamma_0 = 0.06$, both contributions show a strong increase. After this strong increase, the amplitude of the rectangular function is at least a factor of 1.5 larger than the amplitude of the saw tooth function. A large change was also found in the phase lag of both functions at the same value for γ_0. For values of $\gamma_0 < 0.06$, the saw tooth function is approximately in-phase with the linear contribution, whereas the rectangular function is approximately 180° out-of-phase. At $\gamma_0 = 0.06$ the phase of the rectangular function also shows a sudden jump by 120° and is then approximately in-phase with the linear contribution. This happens for a γ_0 value, where a G″ overshoot can be detected in a strain sweep, as in Figure 7. This behavior is consistent with type III behavior according to the classification of Professor Ahn.[9]

Separation of Different Nonlinear Behavior. With the ability to split up the time domain signal into different characteristic contributions, the possibility to separate the linear contribution and the strain softening contribution from the contribution of shear bands or wall slip should be possible. To achieve such a separation of the time domain signal into different contributions, a reconstruction of the time domain signal is first needed. The contributions from the linear response and from the strain softening response are then superimposed. This resulting superimposed signal is afterwards analyzed with respect to the intensities of the higher harmonics and the predicted phases. The higher harmonics of the four characteristic functions are compared with the higher harmonics of the experimental stress function determined directly without any separation via the FT-analysis. As an example, this analysis was performed on samples 1 and 2. The comparison of the magnitudes of the higher harmonics is shown in Figure 10a (sample 1) and in Figure 11a (sample 2), and the phases of the higher harmonics are shown in Figure 10b (sample 1) and Figure 11b (sample 2). The values of the relative magnitude and absolute phase of the third harmonic of sample 1 can very well be reproduced with this new analysis, except only at small γ_0 values where deviations cannot be detected due to small torque values of the measurement. About 20 PS dispersion were synthesized. These monodispers dispersions, varying in diameter, solid content, and ion concentration, showed a similar behavior.

In the case of sample 2, larger deviations in the intensity of the third harmonic (see Figure 11a) are detected. The lower intensities of the third harmonic at small strain amplitudes can be explained by a destructive superposition (destructive interference) of the Fourier contributions of the intensity of the third harmonic originating from the saw tooth function and of the out-of-phase contribution of the rectangular function (see Figure 12). In this plot the time domain contributions and the real part after the Fourier transformation of the sine function (a), of the in-phase rectangular function (b), of the 180° out-of-phase rectangular function (c), and the in-phase saw tooth function (d) are shown. The sine function and the in-phase rectangular function show only positive contributions for the harmonics, whereas the out-of-phase rectangular function shows only negative values for the harmonics. The in-phase saw tooth function shows positive values for the odd harmonics and negative values for the even harmonics. The experimentally measured intensity of the third harmonic could therefore be smaller than the intensity of the strain softening rectangular

Table 8. Amplitude $4/\pi A_r$, $2A_{st}$ and the Phase Values δ_r, δ_{st} of the Rectangular Function and of the Saw Tooth Function[a]

strain amplitude γ_0	normalized rectangular amplitude	rectangular phase [°]	time lag [ms]	normalized saw tooth amplitude	saw tooth phase [°]	time lag [ms]
0.05	0.1	337	936	0.016	239	663
0.1	0.39	338	938	0.014	217	603
0.5	1.54	341	947	0.004	206	572
1	1.74	346	961	0.004	242	672
1.5	1.72	348	967	0.01	225	625
2	1.66	361	1003	0.28	261	725
2.5	1.65	353	981	0.01	228	633
3	1.62	354	983	0.009	240	667
4	1.61	355	986	0.005	288	800

[a] Additionally, the phase lag between the linear response and the rectangular or saw tooth contribution is translated into a time lag. The data sets were acquired at 1 Hz and $0.05 \leq \gamma_0 \leq 4$ from sample 1. The sinusoidal response was used as a reference with the amplitude set to $A_l = 1$ and a phase angle $\delta_l = 0$.

Table 9. Amplitude $4/\pi A_r$, $2A_{st}$ and the Phase Values δ_r, δ_{st} of the Rectangular Function and of the Saw Tooth Function[a]

strain amplitude γ_0	normalized rectangular amplitude	rectangular phase [°]	time lag rectangular [ms]	normalized saw tooth amplitude	saw tooth phase [°]	time lag saw tooth [ms]
0.01	0.34	139	386	0.55	319	886
0.025	0.312	141	391	0.55	329	913
0.05	0.312	138	383	0.42	331	919
0.075	1.11	-4	988	1.06	317	880
0.1	1.3	1	3	1.06	317	880
0.25	1.92	21	58	0.78	336	933
0.5	1.7	39	108	0.53	350	972
1.75	1.58	48	133	0.47	359	997
1	1.4	51	141	0.36	362	6

[a] Additionally, the phase lag between the linear response and the rectangular or saw tooth contribution is translated into a time lag. The data sets were acquired at 1 Hz and $0.01 \leq \gamma_0 \leq 1$ from sample 2. The sinusoidal response was used as a reference with the amplitude set to $A_l = 1$ and a phase angle $\delta_l = 0$.

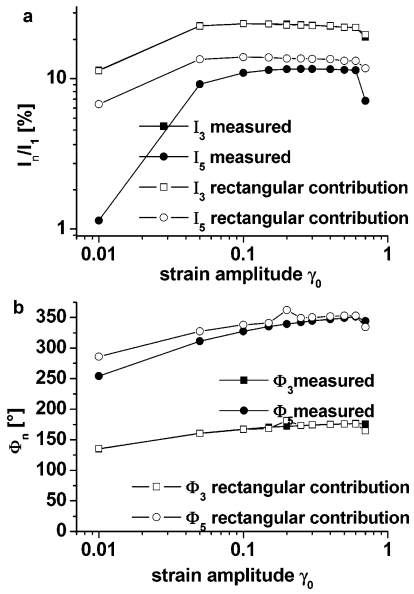

Figure 10. Dependency of the intensity I_n/I_1 and the phase ϕ_n of the third and the fifth harmonic on the strain amplitude of sample 1. The filled symbols show the results from the FT-analysis, and the open symbols show the results corrected for shear band, utilizing the saw tooth function.

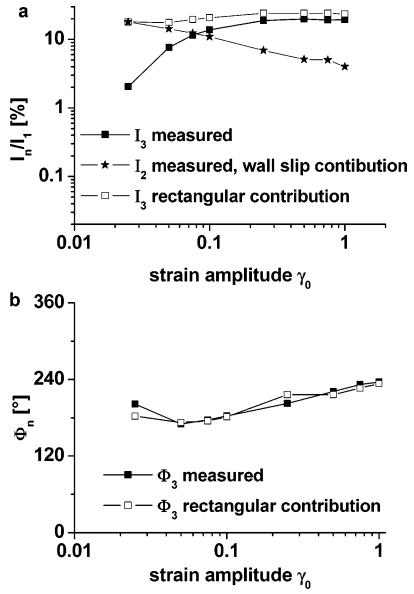

Figure 11. Dependency of the intensity I_3/I_1 and the phase ϕ_3 of the third harmonic on the strain amplitude of sample 2. The filled symbols show the results from the standard analysis, and the open symbols show the results corrected for shear band, respectively the saw tooth function. The star-shaped symbols give the measured values of the intensity of the second harmonic I_2/I_1. In Figure 9a at small γ_0, the intensity of I_3/I_1 is small due to the destructive interference of the third harmonic intensity of the rectangular and saw tooth contribution.

contribution, due to the destructive interference of the intensity of the odd harmonics.

With a different phase shift, an increase of the intensity of the third harmonic I_3/I_1, even larger than the individual contributions, could also be achieved. As an example, the Fourier contributions of the third harmonic from the rectangular function and the saw tooth wave originating from eqs 1 and 2 are repeated:

$$I_3 = A_r \frac{4}{\pi} \frac{\sin 3(\omega t + \delta_r)}{3} + A_{st} 2 \frac{\sin 3(\omega t + \delta_{st})}{3} \qquad (7)$$

The phase of the rectangular function is set for this illustrative example to $\delta_r = 180°$, whereas the phase of the saw tooth function is in-phase, meaning $\delta_{st} = 0°$. This results in

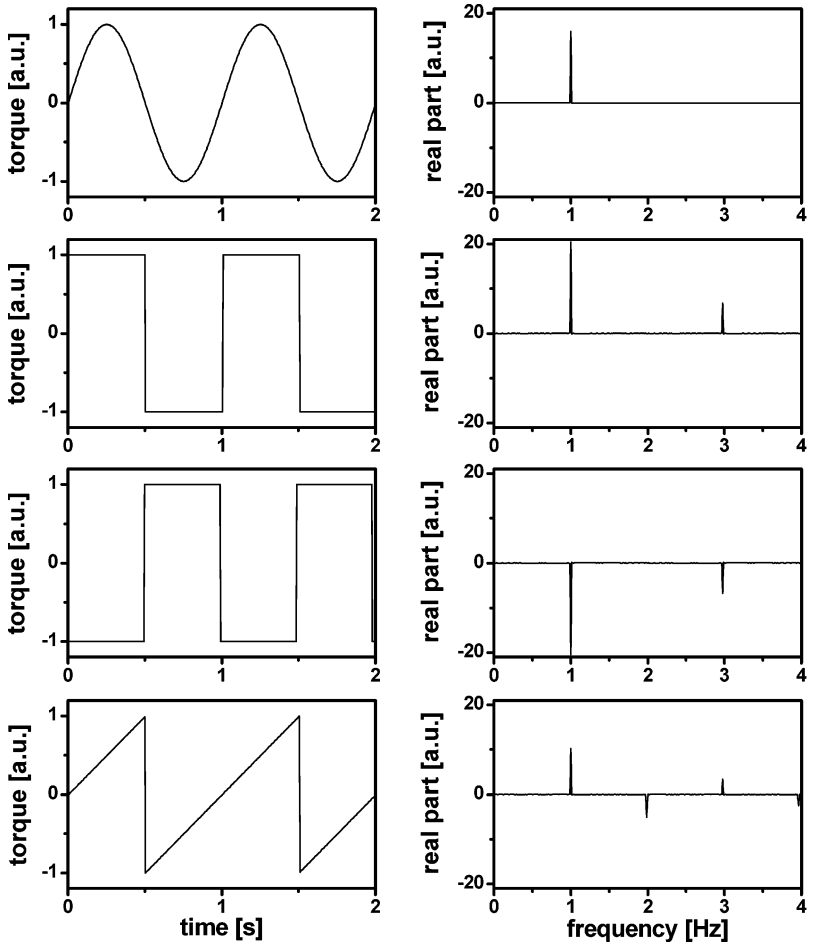

Figure 12. From the top to the bottom, the time domain contributions and the real part after the Fourier transformation of the sine function, the in-phase rectangular function, the out-of-phase rectangular function, and the in-phase saw tooth function are shown. It is clearly visible that the out-of-phase rectangular function has a negative intensity of the third harmonic, whereas the in-phase saw tooth function has a positive intensity of the third harmonic allowing destructive interference.

$$I_3 = A_r \frac{4}{\pi} \frac{\sin 3(\omega t + 180°)}{3} + A_{st} 2 \frac{\sin 3\omega t}{3} \qquad (8)$$

This can even lead to a vanishing intensity of a third harmonic in case of $A_r * 4/\pi = 2\ A_{st}$

$$I_3 = -A_r \frac{4}{\pi} \frac{\sin 3\omega t}{3} + A_{st} 2 \frac{\sin 3\omega t}{3} = 0 \qquad (9)$$

The differences between the measured and the reconstructed phases were negligible (see Figure 11b). With this new data analysis, the high nonlinearities can be separated into the different characteristic contributions of a rheological response in the time and frequency domain. Additionally, the time lag (phase) between the individual contributions is accessible, which could possibly be related to intrinsic time scales. Further examination should focus on the analysis of time domain data at different excitation frequencies.

This new method was first here applied on model dispersions; an extension to more complex systems like polymer solutions, melts, or other complex rheological systems is intended.

Conclusions

In this article, a superposition method to analyze the frequency domain and the time domain signal for LAOS type stress responses was developed. On the basis of the superposition of typical response functions, a sinusoidal, a rectangular, a triangular, and a saw tooth wave, corresponding to the linear contribution, strain softening, strain hardening, and wall slip or shear bands, respectively, the time domain signal is reconstructed. Agreement with the measured time and the frequency domain data was optimized. The advantage of this approach is simplicity because the characteristic functions represent well-known linear and nonlinear rheological response archetypes. As a result, the measured signals can be described by their relative intensities and their relative phases of the harmonics (respective time lag). This new approach was tested for two water-based polymer dispersions as very accurate and promising. This analysis was applied to a set of time domain signals with increasing strain amplitudes. For polystyrene dispersions, it was found that the phase of the rectangular function strain softening is in-phase with the linear contribution, and that the magnitude shows a similar intensity as the third harmonic in the FT-analysis.

Until now the FT-analysis of nonlinear oscillatory mechanical response was focused on the relative intensity of the third harmonic magnitude I_3/I_1 and its phase Φ_3. In cases where the Fourier spectrum exhibits a significant number of higher harmonics, as well as even harmonics at $2\omega_1$, $4\omega_1$, etc. in addition to the odd ones normally observed, this approach is not sufficient. Considering the whole spectrum as resulting from a superposition of characteristic responses, a separation of the sine and rectangular functions from the saw tooth function seems adequate while still keeping simplicity. This approach was applied to samples with intense and reproducible second harmonics I_2. After the separation, the analysis indicated much

larger values for the strain softening contributions of the third harmonic at small strain amplitudes, whereas the values of the phase Φ_3 were like those in the direct FT-analysis of the shear stress. Additionally, destructive interference of the intensity of the third harmonic originating from different contributions was found and could be explained. Thus, this method is indeed able to separate the different contributions and is recommended to analyze samples where intense second harmonic is found.

Acknowledgment. We thank the Deutsche Forschungsgemeinschaft for the financial support (DFG WI 1911/1), the European Union (Marie-Curie Trainingssite IMP HPMT-2000-00188, Marie Curie MEST-CT-2004-513924), and the BMBF-Verbundvorhaben (01RC0175 "Wasser als Medium bei Herstellung, Verarbeitung und Anwendung von Kunststoffen" im Förderschwerpunkt: "Integrierter Umweltschutz in der Kunststoff- und Kautschukindustrie").

References and Notes

(1) Larson, R. G. *The Structure and Rheology of Complex Fluids*; Oxford University Press: Oxford, 1999.
(2) Macosko, C. W. *Rheology: Principles, Measurements, and Applications*; VCH publishers: New York, 1994.
(3) Craciun, L.; Carreau, J. P.; Heuzy, M. C.; Moan, M.; Ven, T. G. M. Rheological properties of concentrated latex suspensions of poly (styrene butadiene). *Rheol. Acta* **2003**, *42*, 410−420.
(4) Giacomin, A. J.; Dealy, J. M. Large-amplitude oscillatory shear. In *Techniques in Rheological Measurements*; Collyer, A.A., Ed.; Chapman and Hall: London, 1993; p 99.
(5) Kallus, S.; Willenbacher, N.; Kirsch, S.; Distler, D.; Neidhoefer, T.; Wilhelm, M.; Spiess, H. W. Characterization of polymer dispersions by fourier-transform rheology. *Rheol. Acta* 2001, *40*, 552−559.
(6) Krieger, I. M. A rheometer for oscillatory studies on nonlinear fluids. *Rheol. Acta* **1973**, *12*, 567.
(7) Wilhelm, M. Fourier-transform rheology. *Macromol. Mater. Eng.* **2002**, *287*, 83−105.
(8) Wilhelm, M.; Maring, D.; Spiess, H. W. Fourier-transform rheology. *Rheol. Acta* **1998**, *37*, 399−405.
(9) Hyun, K.; Kim, S. H.; Ahn, K. H.; Lee, S. J. Large amplitude oscillatory shear as a way to classify the complex fluids. *J. Non-Newtonian Fluid Mech.* **2002**, *107*, 51−65.
(10) Sim, H. G.; Ahn, K. H.; Lee, S. J. Three-dimensional dynamics simulation of electrorheological fluids under large amplitude oscillatory shear flow. *J. Rheol.* **2003**, *47*, 879−895.
(11) Wilhelm, M.; Reinheimer, P.; Ortseifer, M. High sensitivity fourier-transform rheology. *Rheol. Acta* **1999**, *38*, 349−356.
(12) Neidhöfer, T.; Wilhelm, M.; Debbaut, B. Fourier-transform rheology experiments and finite-element simulations on linear polystyrene solutions. *J. Rheol.* **2003**, *47*, 1351−1371.
(13) Dusschoten, D. v.; Wilhelm, M. Increased torque transducer sensitivity via over sampling. *Rheol. Acta* **2001**, *40*, 395−399.
(14) Landfester, K. Polyreactions in miniemulsions. *Macromol. Rapid Commun.* **2001**, *22*, 896.
(15) Israelachvili, J. N. *Intermolecular and Surface Forces*; Academic Press: London, 1992.
(16) Lide, D. R. *Handbook of Chemistry and Physics*; CRC: New York, 1996.
(17) Cho, K. S.; Hyun, K.; Ahn, K. H.; Lee, S. J. A geometrical interpretation of large amplitude oscillatory shear response. *J. Rheol.* **2005**, *49*, 747−758.
(18) Bronstein, I. N.; Semendjajew, K. A. *Taschenbuch der Mathematik*; B. G. Teubner Verlagsgesellschaft: Leipzig, Germany, 1991.
(19) Gradshteyn, I. S.; Ryzhik, I. M. *Table of Integras. Series and Products*; Academic Press Inc.: San Diego, CA, 1992.

MA062441U